

The magnetic field in the Coma cluster

L. Feretti^{1,2}, D. Dallacasa³, G. Giovannini^{1,2}, and A. Tagliani²

¹ Dipartimento di Astronomia dell'Università, Via Zamboni 33, I-40126 Bologna, Italy.

² Istituto di Radioastronomia – CNR, via Gobetti 101, I-40129 Bologna, Italy.

³ Joint Institute for VLBI in Europe, Postbus 2, NL-7990 AA Dwingeloo, The Netherlands

April 24, 2018

Abstract. The polarization data of the radio galaxy NGC4869, belonging to the Coma cluster and located in its central region, allow us to obtain information on the structure of magnetic field associated with the cluster itself. A magnetic field of $\sim 8.5 \mu\text{G}$, tangled on scales of the order of less than 1 kpc, is required to explain the observed fluctuations of the rotation measure. This magnetic field is more than one order of magnitude stronger than the equipartition value obtained for Coma C. This implies that the halo source Coma C may not be at the equipartition. Moreover, the need of efficient reacceleration mechanisms for the electrons radiating in Coma C is stronger. The energy supply to the Coma C radiating electrons is probably provided by the cluster merger process.

1. Introduction

The existence of magnetic field associated with the intergalactic medium in clusters of galaxies is indicated by the diffuse non thermal radio emission (radio halos) revealed in some clusters. It has been independently suggested by the existence of excess Faraday rotation measure of polarized radio emission in radio sources within or behind the cluster (Kim et al. 1991) and from the detection of Inverse Compton hard X-Ray emission (Bazzano et al. 1990). The structure of this magnetic field is presently poorly known. Jaffe (1980) suggested that it has to be tangled on a typical galaxy size, while Crusius-Wätzsel et al. (1990), studying the depolarization in 5 strong double sources, find tangling on a smaller scale (0.5-2 kpc¹). For the Coma cluster of galaxies, Kim et al. (1990) give scale sizes for the magnetic field reversals of 6.5-20 kpc.

Send offprint requests to: L. Feretti

¹ A Hubble constant $H_0 = 100 \text{ km s}^{-1} \text{ Mpc}^{-1}$ is used throughout the paper, which corresponds to a scale of 0.34 kpc/arcsec at the Coma cluster distance

The properties of the Coma cluster magnetic field, can be investigated through the study of the extended radio-galaxy NGC4869 (5C4.81), located near the cluster center, completely embedded within the halo source Coma C. This radio source belongs to the class of Narrow Angle Tail (NAT) radio sources, which represent the most extreme example of the interaction between a radio source and the intracluster medium. A detailed study of this radio galaxy (an elliptical with photographic magnitude 14.9^m at $z = 0.0232$) was performed by us with the VLA, with multiple frequencies and resolutions (Dallacasa et al. 1989; Feretti et al. 1990). The radio structure consists of a faint flat spectrum core, from which two straight short jets originate. They are sharply bent at ~ 1 kpc from the nucleus and produce two tails wrapping each other and probably merging. This structure develops in EW for $\sim 4'$ (75 kpc) with some wide oscillations. Then the tail fades progressively and shows a sharp bend to the North, which is detected only at lower frequencies (Dallacasa et al. 1989). The tail spectrum steepens progressively with the distance from the radio core, and at the source periphery it is considerably steeper ($\alpha \sim 2.0$, with $S \sim \nu^{-\alpha}$) than that of the surrounding regions of the radio halo Coma C (Giovannini et al. 1993).

In this paper we present a study of the polarization properties of this galaxy at 4 different wavelengths. We analyze the trends of the depolarization and rotation measure in the jets and along the first arcmin of the tail, and outline the properties of the depolarizing screen external to the source, i.e. the Coma cluster.

We present the observational details in §2 and the images at the variuos wavelenghts in §3. The multifrequency polarization comparison is given in §4, while in §5 we discuss the scenario emerging from the present results.

2. Observations and data reduction

Observations at 3.6, 6, 18 and 20.5 cm were performed with the Very Large Array (VLA) in 1990 and 1991, in different configurations, with a bandwith of 50 MHz. The

pointing was at RA= $12^h 56^m 58.2^s$, DEC= $28^\circ 10' 50''$, corresponding to the optical and radio nucleus of NGC 4869. In Table 1 we give a summary of the observational parameters.

The flux-density scale and polarization position angle were calibrated by observing 3C286. The scale of Baars et al. (1977) was assumed for the flux density and the integrated polarization position angle of 3C286 was assumed 33° at all frequencies. The on-axis instrumental polarization of the antennas was corrected using secondary calibrators observed with a wide range of parallactic angles. The ionospheric Faraday rotation was corrected assuming that the ionosphere is modelled by a thin sheet at the height of 350 km, with a total electron content as provided by the monitoring station at Boulder (Colorado). The phase calibration was made relative to the secondary calibrators 1308+326 and 1345+125, after editing of bad datapoints.

Images in all Stokes parameters were produced with the NRAO AIPS package following the standard procedure (Fourier inversion, Clean and Restore). Self-calibration (Schwab 1980) was applied to minimise the effects of amplitude and phase uncertainties of atmospheric and instrumental origin. The (u,v) data at the same frequency but from different configurations were first reduced separately, for a consistency check, then added together. At 6 cm, in order to enhance the sensitivity and improve the uv coverage, we used also previous A, B and D array data (Dallacasa et al. 1989).

The images in polarized intensity were obtained as $P=(U^2+Q^2)^{1/2}$, and corrected for the positive bias arising from the previous combination. The polarization angle was derived according to $\theta=0.5 \arctan(U/Q)$.

The images at 3.6 and 6 cm were produced with the same uv range and restored with an identical beam of $2.5''$ (HPBW). The images at 18 and 20.5 cm were made with $HPBW=3''$. The parameters relative to the images (resolution and r.m.s noise) are given in Table 1.

3. Results

The full resolution images are presented in Figs 1 to 4. In all cases the lines indicate the orientation of the electric vector, and their length is proportional to the polarization percentage.

Fig. 1. Polarization image of NGC 4869 at 8.44 GHz. The restoring beam is a circular Gaussian of HPBW = $2.5''$. Contour levels of the total intensity image are $-0.025, 0.025, 0.05, 0.1, 0.2, 0.4, 0.8, 1.5, 2.5$ mJy/beam. The E-vector length is proportional to the polarization percentage: 1 arcsec corresponds to 5%.



Fig. 2. Polarization image of NGC 4869 at 4.84 GHz. The restoring beam is a circular Gaussian of HPBW = $2.5''$. Contour levels of the total intensity image are $-0.04, 0.04, 0.08, 0.15, 0.3, 0.6, 1.2$ mJy/beam. The E-vector length is proportional to the polarization percentage: 1 arcsec corresponds to 6.25%.



Fig. 3. Polarization image of NGC 4869 at 1665 MHz. The restoring beam is a circular Gaussian of HPBW = $3''$. Contour levels of the total intensity image are $-0.12, 0.12, 0.2, 0.35, 0.7, 1.5, 3, 6, 10$ mJy/beam. The E-vector length is proportional to the polarization percentage: 1 arcsec corresponds to 2%.



Fig. 4. Polarization image of NGC 4869 at 1465 MHz. The restoring beam is a circular Gaussian of HPBW = $3''$. Contour levels of the total intensity image are $-0.09, 0.09, 0.18, 0.35, 0.7, 1.5, 3, 6, 10$ mJy/beam. The E-vector length is proportional to the polarization percentage: 1 arcsec corresponds to 2%.

NGC4869 is considerably polarized at 3.6 and 6 cm, all along the structure mapped at these wavelengths, i.e. up to $\sim 80''$ from the core. The polarized emission is rather clumpy, with an increase of the fractional polarization along the tail. The polarization percentage at both frequencies is around 20-25% in the jets, and reaches $\sim 40\%$ at $\sim 70-80''$ from the core. The polarization vector at 3.6 cm is generally “transversal” (*perpendicular*) in the tail (Fig. 1). In the head some structure is associated with the blobs in the jets. A significant amount of polarized emission is associated with the short tail originating from the S-E jet, and the local configuration of the magnetic field seems to be circumferential (Faraday rotation at this frequency is small).

At 6 cm (Fig. 2), the fractional polarization and polarization angle are similar to those observed at 3.6 cm, with the clear evidence of rotation of the polarization angle in some regions.

At 18 cm, polarized emission is detected at the 5-6% level in the head, at the very beginning of the tail and in a few clumps further out. The highest beginning of the tail, and in a few clumps further out. The highest fractional polarization is of $\sim 10\%$ at $\sim 30''$ from the core. At further distance, where the brightness of the tail becomes

Table 1. Logs of observations and image parameters; σ_I is the rms noise in the total intensity image; σ_{UQ} is the rms noise in the Stokes' U and Q images.

Frequency (MHz)	λ (cm)	Date	VLA Config.	Obs. Time (hours)	HPBW (arcsec)	σ_I (mJy/beam)	σ_{UQ} (mJy/beam)
8415	3.6	Nov 90	C	7.1	2.5	0.015	0.012
		Apr 91	D	8.7			
4835	6	Nov 90	C	6.7	2.5	0.023	0.017
		Apr 91	D	6.9			
1665	18	Nov 91	B	8.4	3	0.047	0.038
		Nov 90	C	3.5			
1465	20.5	Nov 91	B	8.4	3	0.030	0.027
		Nov 90	C	7.0			

lower than 0.5 mJy/beam, the detection of polarized flux is noise limited. In this case, an upper limit of $\sim 20\%$ can be placed to the fractional polarization. At 20.5 cm the polarized flux is lower than at 18 cm, with peaks of 7-8%. We note that the fractional polarization detected at 20 cm by Kim et al. (1990) along the tail is always below 1%, because of their observing beam ($\sim 1'$) which is much larger than the structures in polarized emission seen in our images, and therefore their data are severely affected by beam depolarization.

4. Polarization comparison

4.1. Rotation measure

We have derived the rotation measure (RM) of the source using the images at 3.6 and 6 cm. Using these two wavelengths, the maximum detectable RM without ambiguity is 1300 rad m^{-2} . We are confident that the RM computed with these close wavelengths has no ambiguity. This was checked by producing two independent maps for the two different frequencies in the C band, i.e. 4835 and 4885 MHz. Since the orientations of polarization vectors are consistent with each other within a few degrees, the $|\text{RM}|$ must be lower than 500 rad m^{-2} .

Fig. 5 presents a grey scale image of the RM distribution. In the head region, including the nucleus, the southern blob and its short tail, we detect the most negative RM, with $\langle \text{RM} \rangle = -243 \text{ rad m}^{-2}$ and with a dispersion $\sigma_{\text{RM}} = 87 \text{ rad m}^{-2}$. This region is about $15''$ (5 kpc) in size, and is located at the inner region of the optical galaxy (see the radio-optical overlay in Dallacasa et al. 1989). The minimal values of the RM are found in the southern blob. We note that Kim et al. (1994) give for this source, referring to the head, two equally likely values of RM, -349.5 ± 6.5 and $-49.2 \pm 10.5 \text{ rad m}^{-2}$. The first value is

roughly consistent with ours, especially considering that the head region may have been defined differently, because of the very different angular resolution.

At the beginning of the tail, i.e. immediately after the northern jet bend, the RM increases, with an average value in the region of highest surface brightness of $\langle \text{RM} \rangle = -44 \text{ rad m}^{-2}$ and with $\sigma_{\text{RM}} = 135 \text{ rad m}^{-2}$. In the tail continuation, the average RM becomes more negative with $\langle \text{RM} \rangle = -197 \text{ rad m}^{-2}$.



Fig. 5. Grey scale image of the RM distribution between 6 and 3.6 cm.

It is evident from Fig. 5 that the RM shows fluctuations on small scales. Following Leahy (1984), we investigate the scale on which the fluctuations in the RM occur using the function $A(\xi)$, defined as the rms difference in rotation between all points separated by an angle ξ in the map. Thus

$$A(\xi) = \sqrt{\langle (f(\theta) - f(\theta + \xi\phi))^2 \rangle}$$

where θ is a position in the map and ϕ is a unit displacement vector; the average is taken over all θ and all orientations of ϕ . We note that $A(\xi)$ is the square root of the structure function suggested by Simonetti et al. (1984). For a single value of RM with random fluctuations, the rms difference function should increase monotonically with separation until there is no correlation, after which the value of $A(\xi)$ should be $\sigma\sqrt{2}$, where σ is the large-scale standard deviation. The function $A(\xi)$ obtained from our

data is given by the error bars in Fig. 6. The dots in the same figure represent the structure function of the RM noise map.



Fig. 6. Structure function $A(\xi)$ as defined in the text. The bars refer to the RM map, the dots to the RM noise map

The structure function is not influenced by the noise in the RM values. It increases up to about $2.5''$, where it shows a significant change of slope. After this size, it flattens or increases very slowly. The behaviour of the structure function is consistent with the existence of a typical fluctuation size of $2.5''$, with the possible presence of additional fluctuations of larger scale. We note that the smallest size obtained from the structure function corresponds to the beam size, therefore possible smaller fluctuations would not be resolved.

The existence of small-scale fluctuations is confirmed by the behaviour of polarization percentage in maps with increasing resolutions. In Fig. 7, we present the profile of the fractional polarization detected at 3.6 cm along the source tail in the map at full resolution ($2.5''$, solid line) and in a map produced with a resolution of $4''$ and same cellsize (dotted line). The values of the fractional polarization in the lower resolution are systematically lower, indicating significant beam depolarization and confirming the existence of structure of the linearly polarized emission on angular scales between $2.5''$ and $4''$.



Fig. 7. Fractional polarization at 3.6 cm along the ridge of the images restored with a circular Gaussian of $2.5''$ (solid line) and $4''$ (dotted line).

At 18 and 20.5 cm, the orientation of the polarization angle is not consistent with the higher frequency values and a λ^2 law. In the tail, the polarization angle is oriented mostly longitudinally, with a few oscillations on much larger scales than expected by the RM structure. Since the deviations from the λ^2 law could be due to a significant effect of beam depolarization at long wavelengths, we re-examined the 20 cm A-array data presented by Dallacasa et al (1989), to have information with the highest resolution. Unfortunately, no significant polarized flux was detected with the angular resolution of $1''$, due to the noise limitation.

4.2. Depolarization Ratio

We define as depolarization ratio between two wavelenghts λ_1 and λ_2 , with $\lambda_1 < \lambda_2$, the value

$$DP_{\lambda_1}^{\lambda_2} = m(\lambda_2)/m(\lambda_1)$$

where $m(\lambda)$ represents the fractional polarization at the given wavelength. The depolarization ratio between 6 and 3.6 cm, computed using only the values of the polarization percentage with errors $<5\%$, is around 0.8-1 (see Fig. 8), with no evidence of any trend similar to that of the rotation measure. A plot of the rotation measure versus the depolarization ratio (Fig. 9) confirms the lack of any correlation between the two parameters. The source is strongly depolarized at 18 and 20.5 cm. In the few regions where polarized flux is detected, the depolarization ratios with respect to 3.6 cm are around 0.1-0.2.

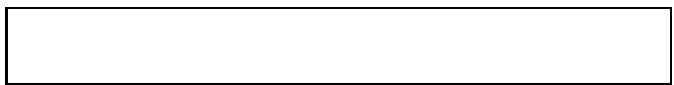


Fig. 8. Depolarization ratio between 6 and 3.6 cm, derived along the ridge of the total intensity emission.



Fig. 9. Plot of rotation measure against depolarization ratio between 6 and 3.6 cm.

5. Interpretation of the polarization data

Laing (1984) warned about the difficulty of interpretation of the polarization data, and indicated the case of deviations from λ^2 rotation associated with depolarization as the hardest to sort out, since the Faraday effect in this case can originate both internally within the source, and in an external foreground screen. We summarize in the following the relevant arguments useful for the interpretation of polarization data.

5.1. Internal Faraday effect

In case that the Faraday effect originates entirely within the source, Burn (1966) predicts that the polarization angle will obey a λ^2 law of rotation and that significant rotation will be accompanied by severe depolarization. Assuming a simple source geometry (slab), the polarization percentage at the wavelength λ , P_λ , is reduced with respect to the intrinsic polarization P_i according to the formula

$$P_\lambda = P_i \frac{\sin(RM\lambda^2)}{RM\lambda^2} \quad (1)$$

while the positon angle χ rotates as λ^2 in the range $0 \leq \chi \leq \pi/2$, and then changes regularly showing a "sawtooth" variation (Laing 1984). In more realistic mixed geometries, P_λ does not have zeroes and the polarization angle will obey a λ^2 rotation over at most 90° .

5.2. External uniform screen

In the simplest case of Faraday depth effectively constant across the beam, the Faraday effect from a screen (single slab) external to the source and with uniform magnetic field produces no depolarization and a rotation of the polarization angle given by $\lambda^2 \langle RM \rangle$, with

$$\langle RM \rangle = 812 B_{\parallel} n_e d \quad (2)$$

where n_e is the electron density in cm^{-3} , B_{\parallel} is the strength of magnetic field along the line of sight in μG , and d is the depth of the screen in kpc.

5.3. External screen with tangled magnetic field

The existence of small scale structure of the magnetic field in an external screen is relevant to produce both rotation of the polarization angle and depolarization. The effect of a Faraday screen with a tangled magnetic field has been analyzed by Lawler and Dennison (1982) and by Tribble (1991). In the simplest ideal case, the screen is made of cells of uniform size, electron density and magnetic field strength, but with field orientation at random angles in each cell. The observed RM along any given line of sight will be generated by a random walk process, and the distribution of the RM results a gaussian with zero mean and variance given by

$$\sigma_{RM} = \frac{812}{\sqrt{3}} n_e B N^{1/2} l \quad (3)$$

where n_e is the electron density in cm^{-3} , B is the magnetic field strength in μG , N is the number of cells along the line of sight and l is the size of each cell in kpc. The depolarization produced by a Faraday screen with tangled magnetic field can be approximated at a long wavelength λ by the formula suggested by Tribble (1991), which includes dependence on the uniform cell size and RM dispersion

$$DP \sim \frac{\theta}{\theta_b} \cdot \frac{0.6}{\sigma_{RM} \lambda^2} \quad (4)$$

where θ is the angular size of each cell and θ_b is the size of the observing beam.

5.4. External screen with tangled magnetic field and gas density distribution

In the case of a tangled magnetic field, the value of σ_{RM} can also be obtained for a more realistic gas density distribution. It has been found that the gas density in clusters

of galaxies follows a hydrostatic isothermal beta model (Cavaliere and Fusco-Femiano 1981), i.e.

$$n_e(r) = n_0 (1 + r^2/r_c^2)^{-3\beta/2} \quad (5)$$

where n_0 is the central electron density, and r_c is the core radius of the gas distribution. In this case, Kim et al. (1991) found

$$\sigma_{RM} = \frac{688B}{(1 + r^2/r_c^2)^{(6\beta-1)/4}} \frac{\Gamma(3\beta - 0.5)}{\Gamma(3\beta)} n_0 M^{1/2} l \quad (6)$$

where M is the number of cells per core radius. For $\beta=0.7$ the previous formula becomes

$$\sigma_{RM} \approx \frac{585B}{(1 + r^2/r_c^2)^{0.8}} n_0 M^{1/2} l. \quad (7)$$

6. Discussion

The observational properties of NGC4869 derived from the polarization data can be summarized as follows:

1. the RM is characterized by the presence of local fluctuations, occurring on typical scales of $\sim 2.5''$. Moreover, it is remarkable that the RM in the head of the source is more negative than in the other regions, with the lowest values in the southern blob;
2. depolarization ratios at 6 cm with respect to 3.6 cm are between 0.8 and 1, while at 18 and 20.5 cm the source is generally much strongly depolarized;
3. the depolarization ratio seem not to be correlated with RM;
4. the orientation of the polarization angle at 18 and 20.5 cm, in the regions where significant polarized flux is detected, shows deviation from a λ^2 law, defined using the angles observed at 3.6 and 6 cm.

We note that the Coma cluster lies close to the north galactic pole, therefore the effect of the interstellar medium of the Milky Way Galaxy on the polarization is negligible.

In NGC4869 the RM distribution is not correlated with the depolarization ratio and this favours the idea that the Faraday effect is mostly external to the source. In this case the deviation from the λ^2 law at long wavelength would be due to beam depolarization. This is consistent with the existence of irregularities in the foreground screen smaller than the observing beam at 20.5 cm.

6.1. Effect of the galaxy NGC 4869

The RM in the head of the source could be affected by the interstellar medium of the galaxy NGC 4869, as already found in the radio galaxy NGC 6047 (Feretti & Giovannini 1988).

However, the scale of the RM fluctuations in the head is not different from that in the tail and also the depolarization of the head is very similar to that in the other

source regions. Therefore, we do not have a definite evidence of the existence of magnetic field associated with the interstellar medium of the galaxy. In any case, since this magnetic field does not seem to affect the dispersion of the RM values, it should be ordered on scales comparable to the galaxy size.

We note that the southern blob in NGC 4869 exhibits a more negative RM than the northern one, and this could arise from the jet orientation. The northern jet is approaching the observer, while the southern one is receding from us (Feretti et al. 1990).

6.2. Effect of the halo Coma C with an ordered magnetic field

The existence of magnetic field associated with the Coma intergalactic medium is directly deduced from the presence of the the diffuse radio halo Coma C, which is permeating the central region of the Coma cluster, for a total size of 25' (Giovannini et al. 1993), corresponding to ~ 500 kpc. No polarization data of Coma C are available to get direct information on the magnetic field structure. The equipartition magnetic field of the halo is $0.5 \mu\text{G}$ (Giovannini et al. 1993). According to X-ray data (Hughes 1988), the gas density distribution follows an hydrostatic isothermal model with central gas density $n_0 = 3.7 \times 10^{-3} \text{ cm}^{-3}$, core radius = 9.8' (corresponding to 198 kpc) and $\beta = 0.76$. According to the orbit computed by Feretti et al. (1990), NGC 4869 is imbedded within the halo, and not simply projected onto it. Assuming equipartition conditions for the halo, i.e. a magnetic field along the line of sight = $0.5 \mu\text{G}$, and that the magnetic field is completely ordered, a rotation measure $|\text{RM}| \approx 300 \text{ rad/m}^2$ is implied (equation 2), constant across the source. While the value of the average RM can be different, depending on the Faraday depth through the cluster, the implication of a constant value across the source is not consistent with our data, given the large detected dispersion in the values of RM.

6.3. Effect of a cluster tangled magnetic field

The dispersion of RM observed across NGC 4869 can be explained by assuming that the magnetic field is tangled on typical scales of the same size as the RM fluctuations, i.e. $2.5''$, corresponding to 0.85 kpc. This leads to ~ 235 cells per cluster core radius. Moreover, field reversals must take place. The RM distribution, obtained using only the values of the polarization angle with errors $<10^\circ$, gives $\langle \text{RM} \rangle = -127 \text{ rad m}^{-2}$, with a dispersion $\sigma_{\text{RM}} = 181 \text{ rad m}^{-2}$. Using the equation (6), assuming a projected distance of 5' from the cluster center, we obtain a magnetic field associated with the intergalactic medium $B = 8.5 h_{100}^{1/2} \mu\text{G}$, where $h_{100} = H_0/100 \text{ km s}^{-1} \text{ Mpc}^{-1}$. This value refers to the trivial case that the projected distance from the cluster center coincides with the true distance. Projec-

tion effects obviously may play an important role. A displacement of NGC4869 from the cluster center also along the line of sight by about $\pm 3.5'$ (see Feretti et al. 1990), leads to an uncertainty of about $\pm 1.5 \mu\text{G}$ on the value of the magnetic field.

With the assumptions of a tangled magnetic field, the expected depolarization ratios at 18 and 20.5 cm, estimated with equation (4), are $\lesssim 0.08-0.06$, roughly consistent with the observational result.

However, a Faraday screen with a tangled magnetic field should produce, as noted in §5.3, a RM distribution with zero mean, which is not the case. Therefore, we have to assume a more complex scenario to explain our data.

6.4. A tangled magnetic field plus a uniform disk

The non zero average RM could be due to the existence of a weak magnetic field component, ordered on a large scale, as suggested by Taylor and Perley (1993) for the source Hydra A. The average RM in the tail is $\langle \text{RM} \rangle = -127 \text{ rad m}^{-2}$, which leads to a magnetic field component ordered on a scale of ~ 200 kpc, with strength of $B=0.1-0.3 \mu\text{G}$, depending on the location of the galaxy along the line of sight.

Kim et al. (1990) and Kim et al. (1994), in a survey of the Coma cluster, obtained Faraday rotation measures of 18 sources at different projected distances from the cluster center and found a significant contribution to the RM of sources seen through the cluster. The sources within 15' from the cluster center, besides our source, are: 5C4.70, 5C4.74 and 5C4.85, which have RM of 47 ± 7 , -65 ± 7 and $-32 \pm 10 \text{ rad m}^{-2}$, respectively. These values of RM are significantly different from the average RM of the present source NGC4869. We note, however, that 5C4.70 and 5C.74 are at more than one core radius from the cluster center, therefore we must consider different Faraday depths, deriving from lower electron densities. The discrepancy between the the average RM of our source, and the value of the RM of 5C4.85, identified with the dominant galaxy of the Coma cluster, could arise from projection effects, and would therefore imply that NGC4869 is actually located beyond NGC4874. Moreover, a contribution from internal origin to the RM of NGC4874 could be present. New high resolution and sensitivity observations would be needed to clarify this point.

6.5. The Coma magnetic field and implications on the conditions of the halo Coma C

The RM value and distribution of NGC4869 can be reasonably explained assuming a two-component magnetic field, one tangled on the kpc scale, the other organized over a scale of 200 kpc. The tangled magnetic field has a strength of about $8.5 \pm 1.5 \mu\text{G}$, while the uniform component is much weaker, about $0.2 \pm 0.1 \mu\text{G}$.

A magnetic field of several μG , associated with the intergalactic medium of clusters of galaxies, is not surprising. The existence of cluster magnetic field is discussed in many recent papers (Ge & Owen 1993, Taylor & Perley 1993, Taylor et al. 1994, Ge & Owen 1994). Generally these cases refer to clusters with cooling flow, where the magnetic field is suggested to be amplified by compression and inflow (Soker & Sarazin 1990). The strength of the magnetic field has been observed to be up to $\sim 30 \mu\text{G}$. The Coma cluster is the first case of a cluster without the cooling flow, where the existence of a magnetic field of several μG is suggested.

Even allowing for the uncertainties related with projection effects, the Coma magnetic field derived in Sect. 6.3 is more than one order of magnitude larger than the value ($B_{eq} = 0.5 \mu\text{G}$) derived by Giovannini et al. (1993), by integrating the total luminosity of the source between 10 MHz and 1 GHz, with a spectral index $\alpha=0.5$ (the low frequency one), assuming energy equipartition between magnetic field and relativistic particles, a filling factor $\Phi = 1$ and equal energy in electrons and heavy particles ($k=1$). We note that the ratio between the magnetic field derived from RM arguments, and the minimum equipartition value is weakly affected by the assumed value of the Hubble constant. Infact, since the equipartition magnetic field scales as $H_0^{2/7}$, the ratio B/B_{eq} depends on $H_0^{3/14}$ (i.e. the ratio only decreases from 17 to 15 if $H_0=50$ is used instead of $H_0=100$).

The large difference between the magnetic field estimated here and B_{eq} could be explained, without abandoning the equipartition hypothesis, assuming a low filling factor ($\Phi < 1$) and a large ratio between the proton and electron energy ($k > 1$). Possible values of the two parameters, whose combination raises the equipartition magnetic field to $8.5 \mu\text{G}$ are given in Table 2.

Table 2. Values of the proton to electron energy ratio k , and of the filling factor Φ needed to raise the equipartition magnetic field to $8.5 \mu\text{G}$.

k	ϕ
1	5×10^{-5}
10	2.7×10^{-4}
10^2	2.5×10^{-3}
4×10^2	1×10^{-2}
1×10^3	2.5×10^{-2}
4×10^3	0.1
1×10^4	0.25
4×10^4	1

We derive that values of k between 10 and 100 (see Feretti et al. 1992 and references therein) imply very low

filling factors. Therefore, we favour the possibility that Coma C is not at the equipartition.

In any case, the total energy content in Coma C is not minimum, but at least 100 times larger than the minimum equipartition value. This would in turn produce a larger internal pressure, thus partly reducing the apparent imbalance between internal non-thermal pressure and external pressure of the X-Ray gas.

The high energy content of the radio halo Coma C has important implications on the physics of this puzzling source. Owing to the large value of the magnetic field, the time for synchrotron radiation losses of electrons in the halo is reduced by at least one order of magnitude, thus reinforcing the need for reacceleration processes. The energy required to sustain the radio emission from the halo is very large and the contribution of galactic wakes in supplying energy from turbulence is not enough to support the existence of Coma C (see Giovannini et al. 1993). From the X-ray map (Briel et al., 1992), it is evident that the Coma cluster is not yet relaxed. Therefore the energy available from the merger process (Tribble 1993) of the NGC 4839 sub-group (Briel et al., 1992) into the main cluster becomes very important for the energy supply of Coma C (Giovannini et al., 1993, Burns et al., 1994). Since thermal and non thermal particles are mixed inside Coma C, we can reasonably assume that for the same reason the Coma magnetic field and relativistic particles are not yet at the equilibrium (equipartition energy condition).

7. Conclusions

The main conclusions of this paper are the following:

1. The large dispersion of the RM distribution of the source NGC 4869 can be interpreted as originating from a cluster magnetic field of $8.5 \mu\text{G}$, tangled on scales of less than 1 kpc. Large magnetic fields have been so far found in clusters showing a cooling flow. This is the first case of a large magnetic field associated with a cluster without a cooling flow.
2. The non zero average of the RM suggests the presence of a weaker magnetic field component, of $0.2 \mu\text{G}$, uniform on a cluster core radius scale (~ 200 kpc).
3. The value of the magnetic field derived in the Coma cluster is more than one order of magnitude larger than the minimum equipartition value computed for the halo source Coma C. This implies that the radio halo is likely to be out of energy equipartition and reinforces the need for reacceleration processes for the relativistic electrons radiating in Coma C. The energy supply in Coma C is likely to be the merger process.

Acknowledgements. We thank R. Fanti for useful suggestions and discussions and M. Bondi for his help with the structure function. We are grateful to P. Kronberg, the referee, for helpful comments. The National Radio Astronomy Observatory

(NRAO) is operated by Associated Universities, Inc., under contract with the National Science Foundation.

References

Baars, J.W.M., Genzel, R., Pauliny-Toth, I.I.K., Witzel A., 1977, *A&A*, 61, 99

Bazzano, A., Fusco-Femiano, R., Ubertini, P., Perotti, F., Quadrini, E., Court, A.J., Dean, A.J., Dipper, N.A., Lewis, R., Stephen, J.B., 1990, *ApJ* 362, L51

Briel, U.G., Henry, J.P., Böhringer, H., 1992, *A&A*, 259, L31

Burn, B.J., 1966, *MNRAS*, 133, 67.

Burns, J.O., Roettiger, K., Ledlow, M., Klypin, A., 1994, *ApJ* 427, L87

Cavaliere, A., Fusco-Femiano, R., 1981, *A&A*, 100, 194.

Crusius-Wätzels, A.R., Biermann, P.L., Lerche, I., Schlickeiser, R., 1990, *ApJ*, 360, 417.

Dallacasa, D., Feretti, L., Giovannini, G., Venturi, T., 1989, *A&A Suppl. Ser.*, 79, 391.

Feretti, L., Giovannini, G., 1988, *A&A*, 191, 21.

Feretti L., Dallacasa D., Giovannini G., Venturi T., 1990, *A&A*, 232, 337.

Feretti, L., Perola, G.C., Fanti, R.: 1992, *A&A*, 265, 9

Ge, J.P., Owen, F.N., 1993, *AJ*, 105, 778

Ge, J.P., Owen, F.N., 1994, *AJ*, 108, 1523

Giovannini, G., Feretti, L., Venturi, T., Kim, K.-T., Kronberg, P.P., 1993, *ApJ*, 406, 399.

Hughes J.P., Gorenstein P., Fabricant D., 1988, *AJ*, 293, 102.

Hughes J.P., 1989, *ApJ*, 264, L65.

Jaffe, W., 1980, *ApJ*, 241, 925.

Laing, R.A., 1984. "Interpretation of radio polarization data" in *Physics of Energy Transport in Extragalactic Radio Sources*, Bridle A.H. and Eilek J.A. eds., NRAO workshop n.9, p.90.

Lawler, J.M., Dennison, B., 1982, *ApJ*, 252, 81.

Kim, K.T., Tribble, P.C., Kronberg, P.P., 1991, *ApJ*, 379, 80.

Kim, K.-T., Kronberg, P.P., Dewdney, P.E., Landecker, T.L., 1990, *ApJ*, 355, 29.

Kim, K.-T., Kronberg, P.P., Dewdney, P.E., Landecker, T.L., 1994, *A&AS*, 105, 385.

Leahy, J.P., 1984, *MNRAS* 208, 323.

Schwab, F.R., 1980, *Soc. Photo-Opt. Instrum. Eng. Proc.*, 231, 18.

Simonetti, J.H., Cordes, J.M., Spangler, S.R., 1984, *ApJ*, 284, 126.

Soker, N., Sarazin, C.L., 1990, *ApJ*, 348, 73

Taylor, G.B., Perley, R.A., 1993, *ApJ*, 416, 554.

Taylor, G.B., Barton, E.J., Ge, J.P., 1994, *AJ*, 107, 1942

Tribble, P.C., 1991, *MNRAS*, 250, 726.

Tribble, P.C., 1993, *MNRAS*, 263, 31.

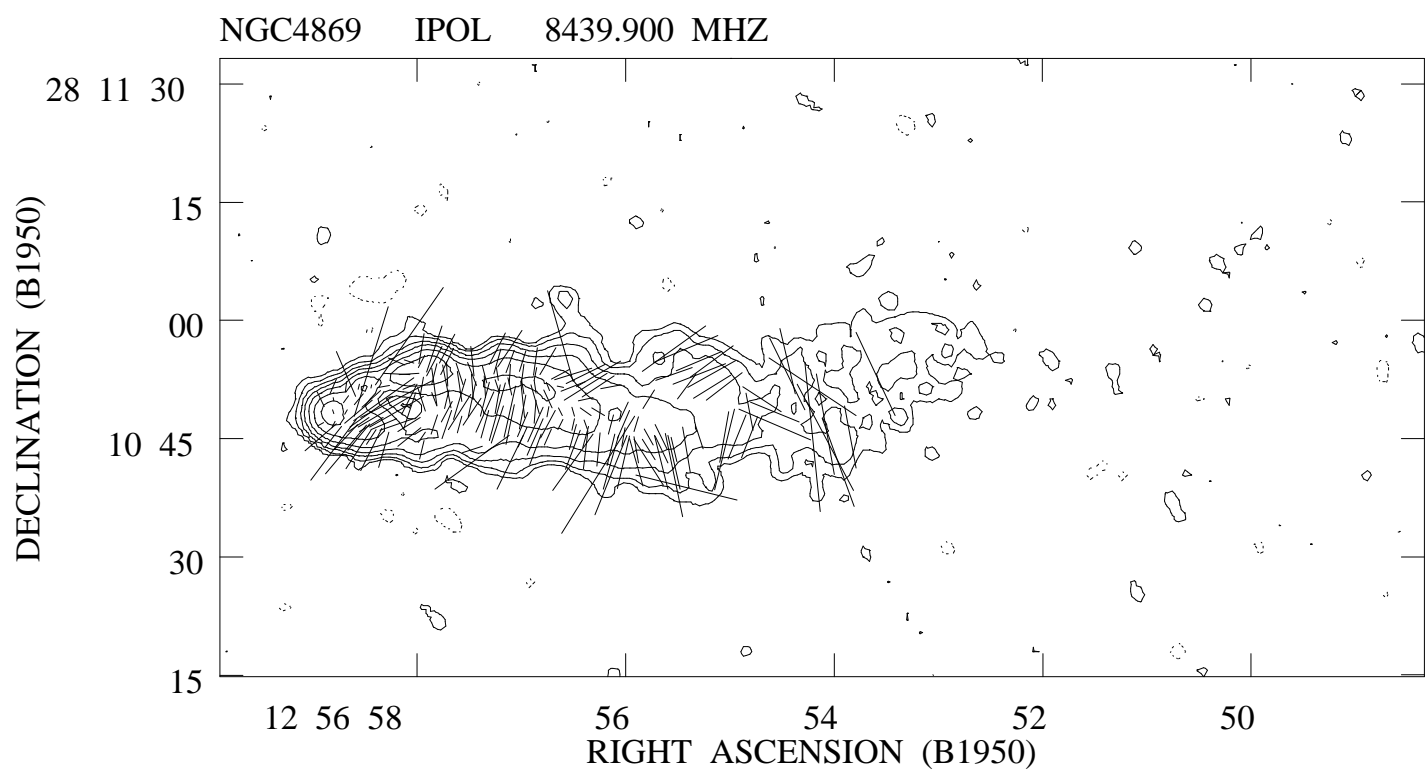


FIGURE 1

DECLINATION (B1950)

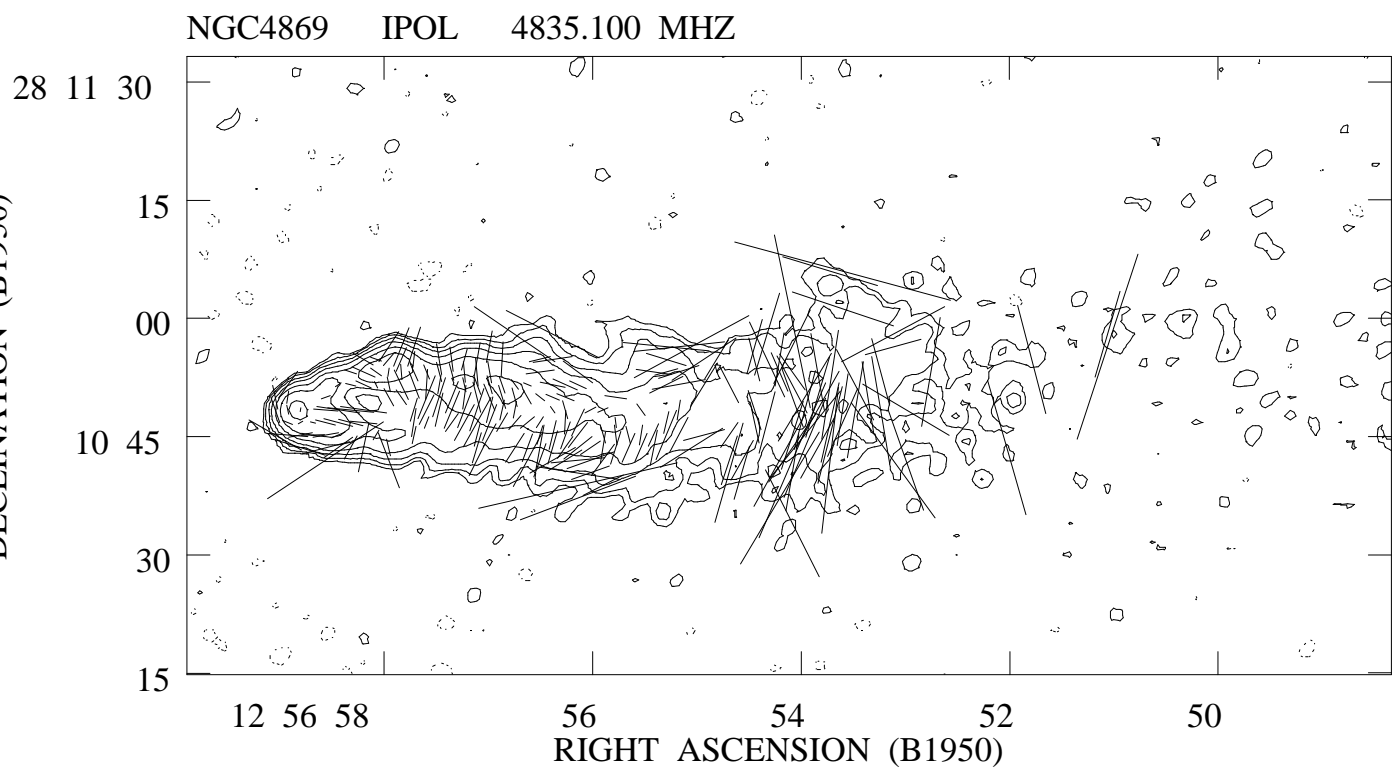


FIGURE 2

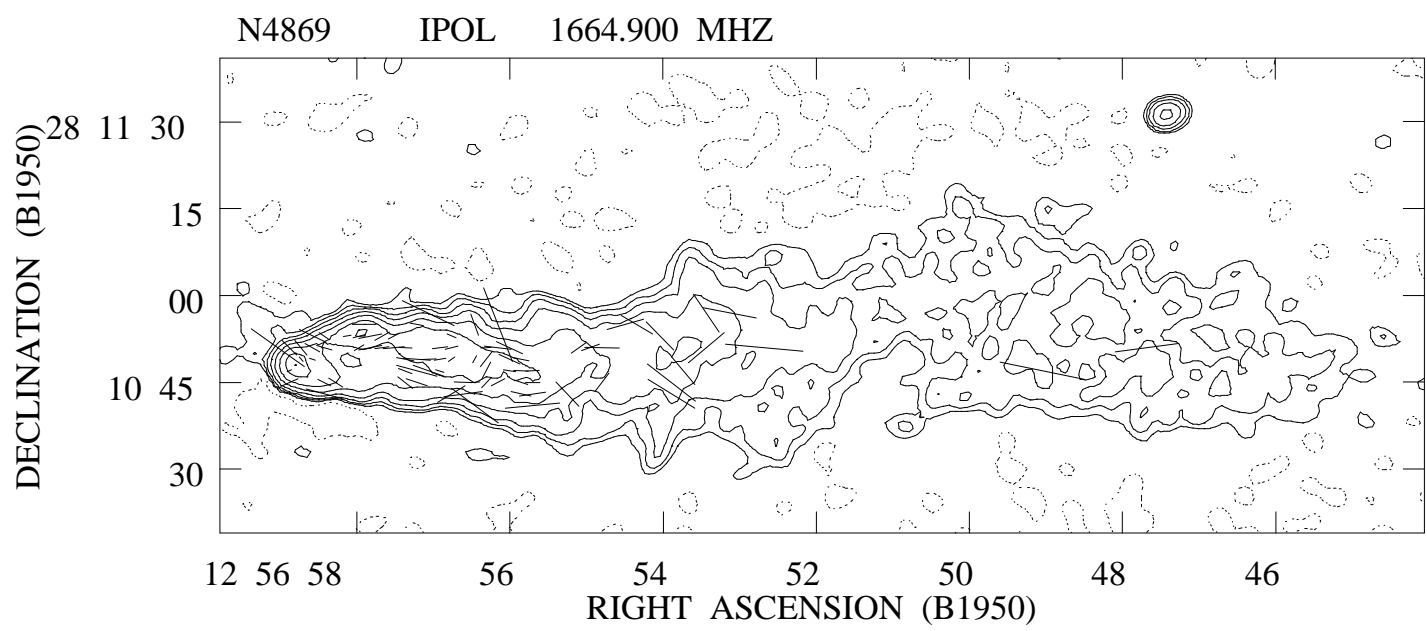


FIGURE 3

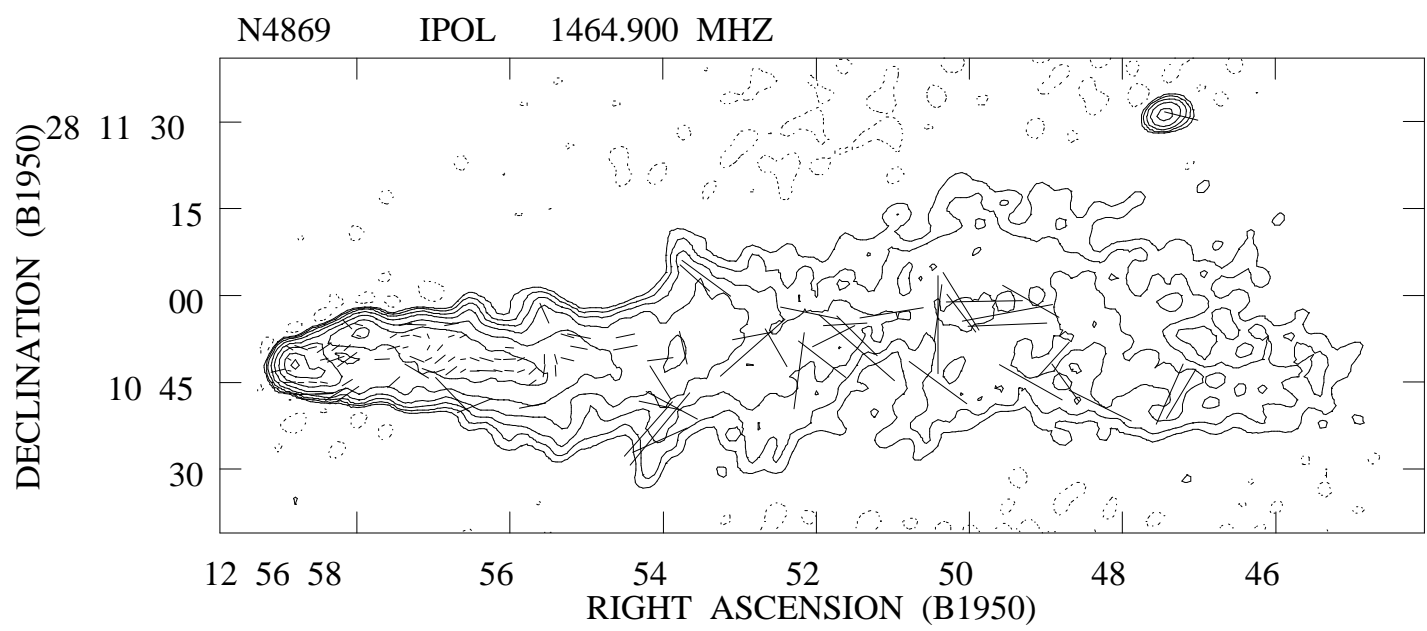


FIGURE 4

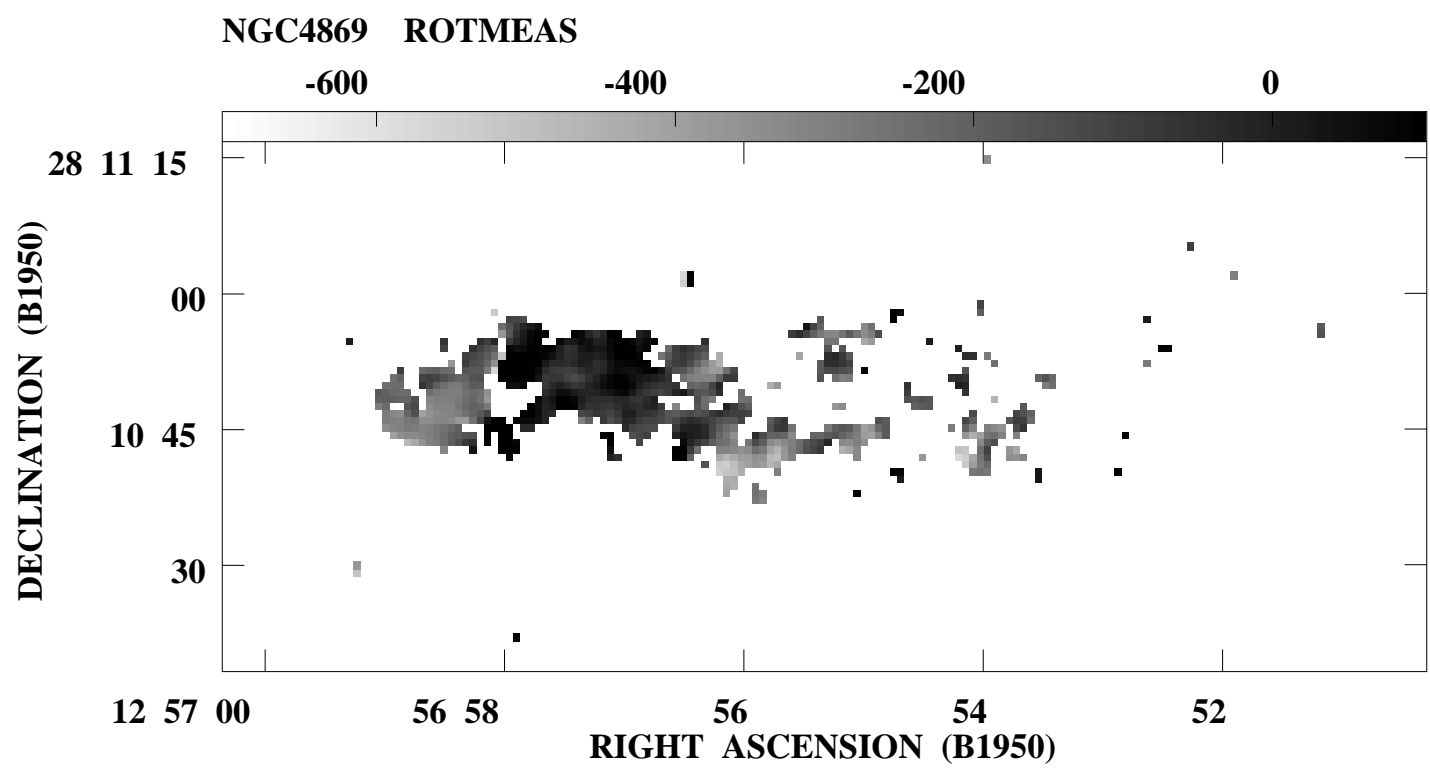


FIGURE 5

FIGURE 6

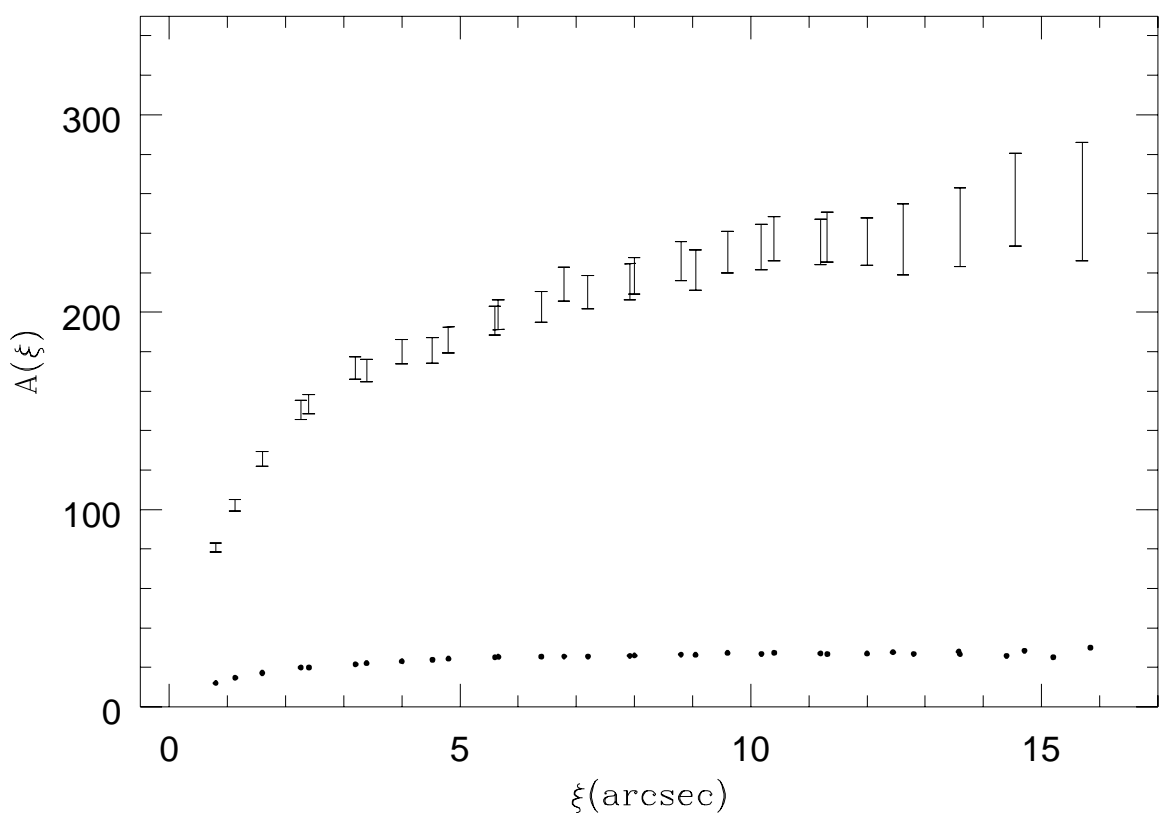
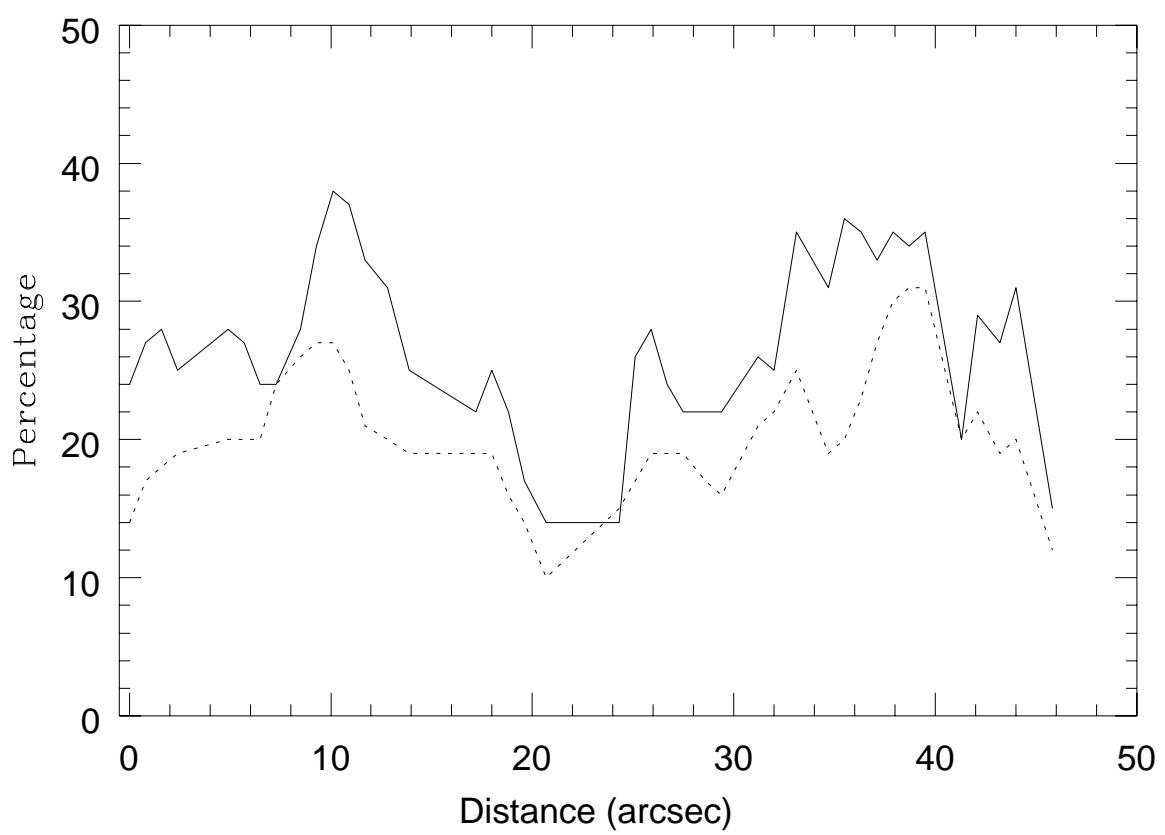


FIGURE 7



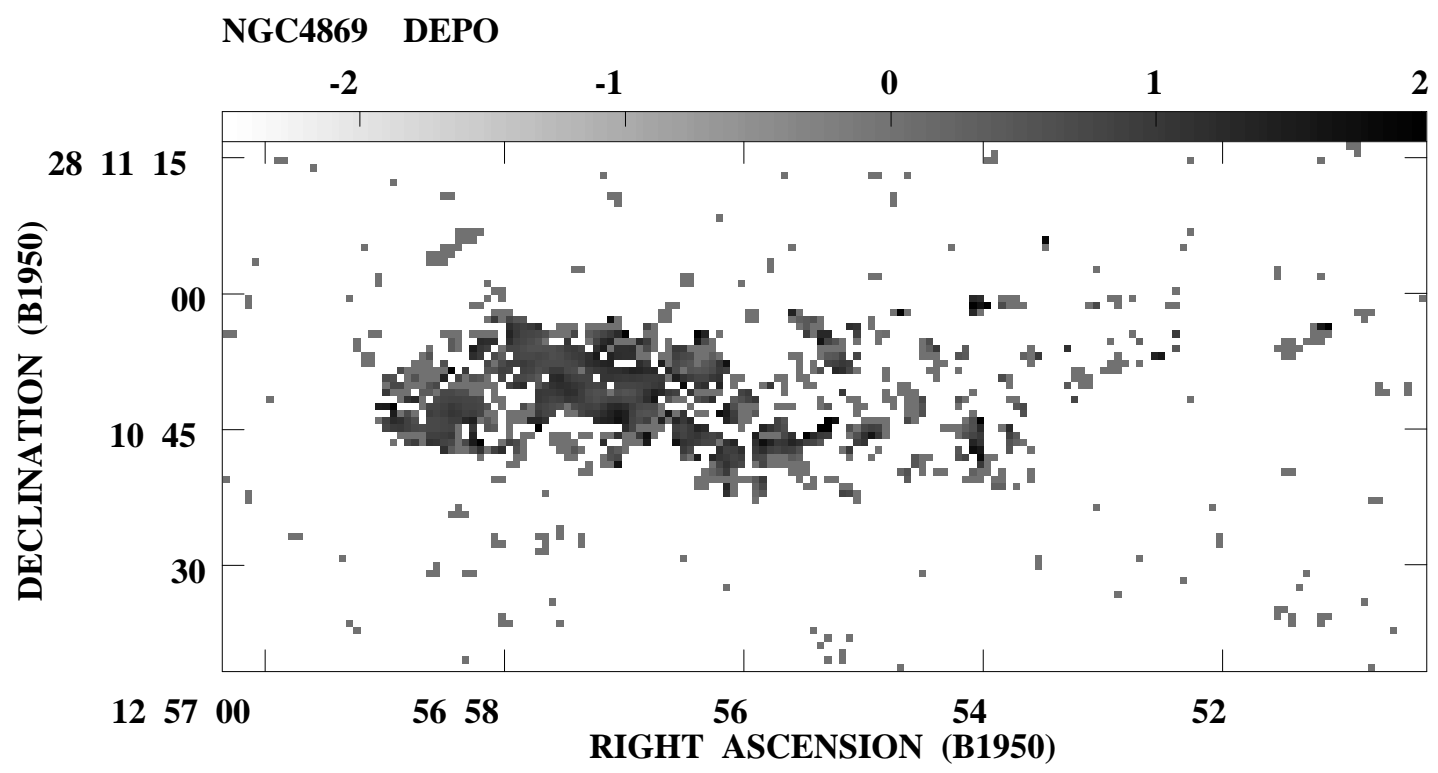


FIGURE 8

FIGURE 9

